ISSN: 1231-4005
e-ISSN: 2354-0133
DOI: 10.5604/01.3001.0012.4807

MODELLING OF A PERMANENT MAGNET MOTOR WITH AN INVERTER IN A DRIVE SYSTEM OF A CAR – PART II

Zbigniew Pawelski, Grzegorz Uszpolewicz

Lodz University of Technology
Department of Vehicles and Fundamentals of Machine Design
Stefanowskiego Street 1/15, 90-537 Lodz, Poland
tel.: +48 42 6312393
e-mail: k-111@adm.p.lodz.pl

Abstract

The article presents a mathematical model of a permanent magnet motor, powered by a three-phase source of sinusoidal voltage, and a control method. Cooperation between numerical integration algorithms in the differential equation system of the motor and an inverter has been verified. The results of numerical simulations are presented in a graphic form. This article is an extension of the publication [12], in which a model of a drive system was proposed, consisting of: a battery, a supercapacitor and a method of controlling these energy sources during a driving cycle of a vehicle. For vector control, the mathematical model of a synchronous machine in the dq coordinate system is the most common one. The most important feature of this control method is the fact that the i_q component of the rotor current vector determines the value of motor torque, and the component i_d – the value of magnetic flux. In the article, the emphasis is put on how inverters work. Their basic task is to generate such currents i_{abc} or voltages u_{abc} to obtain torque without ripples. It leads to development of different control concepts for achieving this goal, which are related to the modelling of magnetic fluxes in a stator and in an inverter.

Keywords: *electrical machines, permanent magnet motor, inverter, electric drive control system*

1. Inverter model

The motor should be powered by phase current changing in relation to the angle θ_e, in order to reduce electromagnetic torque ripples. An exemplary design of the motor and ideal production of sinusoidal current (i_{abc}) or voltage (u_{abc}) by the inverter should result in torque without any ripples. In practice, however, there are some torque ripples and vibrations. Generally, modelling and controlling with high accuracy cannot suppress ripples, which forces the development of various control concepts.

In the case of powering from the grid through a diode rectifier, the capacitor C_F is charged in the DC circuit, Fig. 1, connecting the rectifier with the transistor converter. The larger the capacity of the capacitor, the smaller the changeability of the DC voltage, but the higher costs and the bigger size of the capacitor, as well as the greater unfavourable influence of the rectifier currents on the external network, exceeding the level allowed by the standards. The induction coil L_F suppresses the peak current [11].

Typical configurations of PWM converter consist of three half-bridges, one for each phase, Fig. 1. The inverter transforms DC busbar voltage into multiphase AC voltage with expected frequency. The course of phase voltage is depicted in Fig. 2e.

In order to obtain three-phase output voltage with PWM, the triangular voltage signal u_t is compared with three sinusoidal controlling signals u_a, u_b and u_c with assumed frequency and moved by 120º, Fig. 2a [11]. For example, when u_a is higher than u_t then S1 is closed and S4 is open, Fig. 1. When the voltage u_a is lower than u_t, S4 is closed and S1 is open. The ultimate course of phase voltage u_{aN} is shown in Fig. 2b. In a similar way, the phase voltages u_{bN} and u_{cN} are described by comparing the voltages u_b and u_c with the voltage u_t for the switches S3, S6 and S5,

S2. The obtained voltages u_{bN} and u_{cN} are moved by 120º and 240º, Fig. 2c and Fig. 2d. The voltages u_{aN}, u_{bN} and u_{cN} are measured with respect to the negative DC busbar.

The value of voltage u_{ab} is determined by subtracting the voltage u_{bN} from the voltage u_{aN}. The courses of momentary voltages and *rms* are depicted in Fig. 2e.

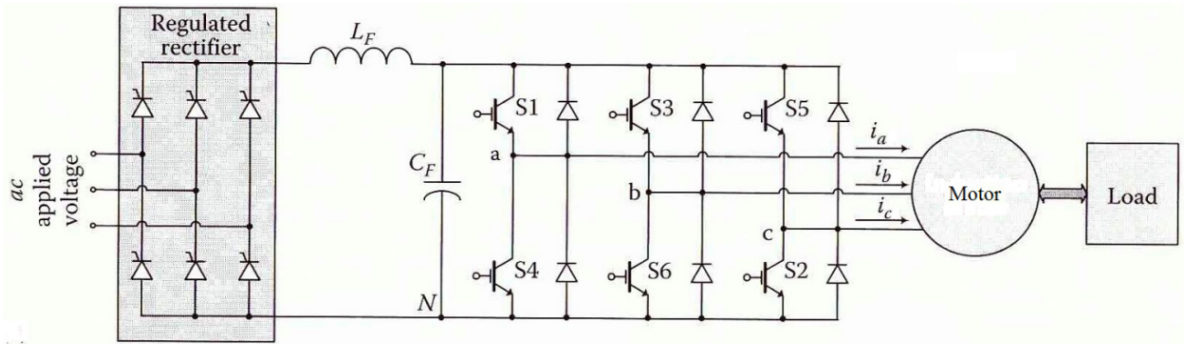

Fig. 1. Power converter with a three-phase hard switch [11]

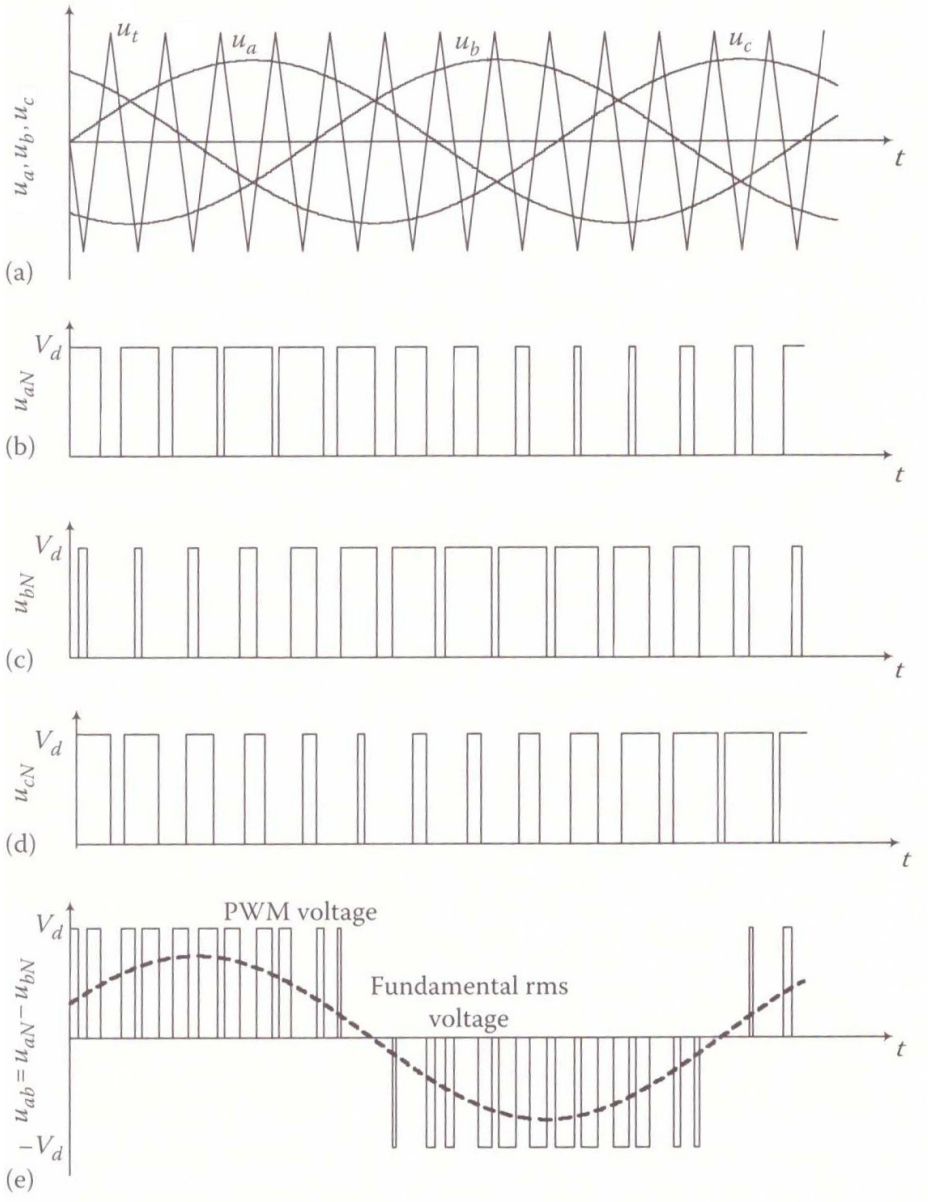

Fig. 2. Courses of voltages in a three-phase inverter [11]

During basic work of inverters, each switch is closed for 180º and open for the other 180º, cyclically. Moreover, S3 is closed 120º after closing S1, S5 is closed 120º after closing S3, S4 – 120º after S2, S6 – 120º after S4, S2 – 120º after S6, Fig. 3. The result is a combination of three keys closed simultaneously after each 60º.

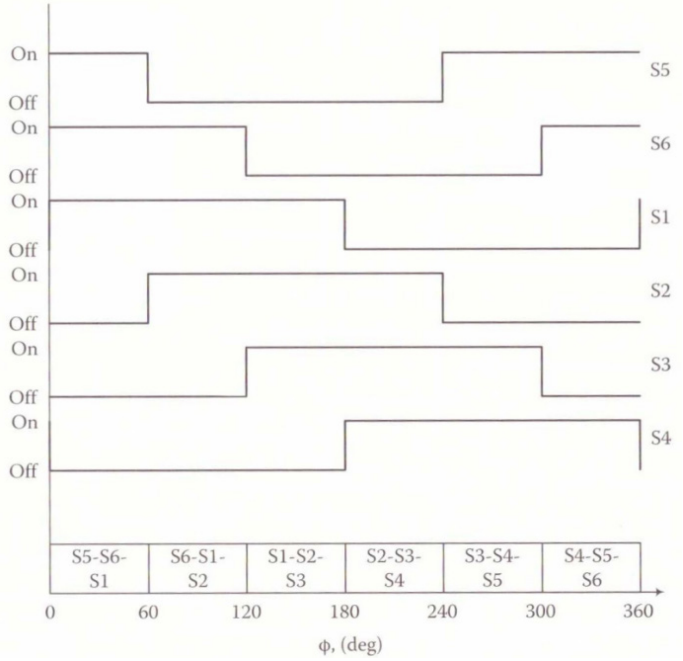

Fig. 3. Scheme of switching in six-step three-phase inverters [11]

In a time interval between 0 and 60º, when switches S5, S6 and S1 are closed, the phase *a* and the parallel phase *c* are connected in a serial way to the phase *b*, which is connected to the power source through S6. At a voltage jump, e.g. $u_{aN} = u_{cN} = V_d$, we receive $u_{bN} = 0$, $u_{ab} = V_d$, $u_{bc} = -V_d$, $u_{ca} = 0$. Because the phases *a* and *c* are parallel, the apparent impedance with respect to the motor star point (*N* point) is half-lower. Therefore, a voltage drop in a phase is always $1/3V_d$ or $2/3V_d$, depending on the connection between the phases *a*, *b* and *c*: series or parallel [11].

For current converters, Fig. 4, the concept of action changes. The inverter is powered from a direct current source. The task of the high inductance *L* in DC is to minimalize the current pulsation. In each moment, there are only two thyristors working – one is connected to the positive circuit and the other is connected to the negative circuit. Current is switched in sequences to one of the three-phase motor phases through "the upper half of the inverter". It comes back from a different phase through "the lower half of the inverter" to the direct current link. There is a permanent voltage drop in the stator winding depending on the resistance of the winding.

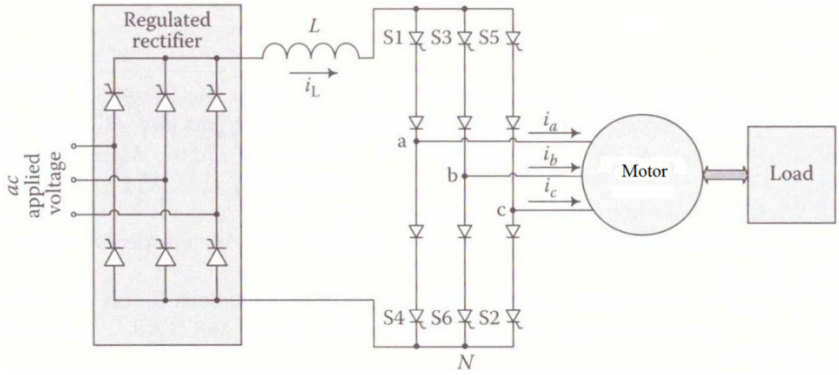

Fig. 4. Converter with a current source and thyristors [11]

A common practise in controlling inverters is using the mathematical transformation $\alpha,\beta,0$, known as Clarke transformation, because it simplifies the analysis of three-phase circuits and allows generating a signal used to control the modulation of spatial vectors in inverters of three-phase drives. In the transformation, it is justifiable to use [7]:

$$\begin{bmatrix} u_\alpha \\ u_\beta \\ u_0 \end{bmatrix} = \begin{bmatrix} \frac{2}{3} & -\frac{1}{3} & -\frac{1}{3} \\ 0 & \frac{1}{\sqrt{3}} & -\frac{1}{\sqrt{3}} \\ \frac{1}{3} & \frac{1}{3} & \frac{1}{3} \end{bmatrix} \begin{bmatrix} u_a \\ u_b \\ u_c \end{bmatrix}, \quad \begin{bmatrix} u_a \\ u_b \\ u_c \end{bmatrix} = \begin{bmatrix} 1 & 0 & 1 \\ \frac{1}{2} & \frac{\sqrt{3}}{2} & 1 \\ -\frac{1}{2} & -\frac{\sqrt{3}}{2} & 1 \end{bmatrix} \begin{bmatrix} u_\alpha \\ u_\beta \\ u_0 \end{bmatrix}. \tag{1}$$

Similar formulas apply to currents. The voltages u_α, u_β and the currents i_α, i_β are orthogonal components of the spatial vectors of voltage **U** and current **I**, which are the same for the motor and the inverter, Fig. 5. The three-phase connection is the cause why the zero-current component i_o, as an arithmetic mean of phase currents, is always 0, and zero-voltage components u_o do not affect phase-to-phase voltages. Considering this, the foregoing formulas are used to describe the phase-to-phase voltages u_{ab} and u_{bc} as follows:

$$\begin{bmatrix} u_\alpha \\ u_\beta \end{bmatrix} = \begin{bmatrix} \frac{2}{3} & -\frac{1}{3} \\ 0 & \frac{1}{\sqrt{3}} \end{bmatrix} \begin{bmatrix} u_{ab} \\ u_{bc} \end{bmatrix}, \quad \begin{bmatrix} u_{ab} \\ u_{bc} \end{bmatrix} = \begin{bmatrix} \frac{3}{2} & -\frac{\sqrt{3}}{2} \\ 0 & \sqrt{3} \end{bmatrix} \begin{bmatrix} u_\alpha \\ u_\beta \end{bmatrix}. \tag{2}$$

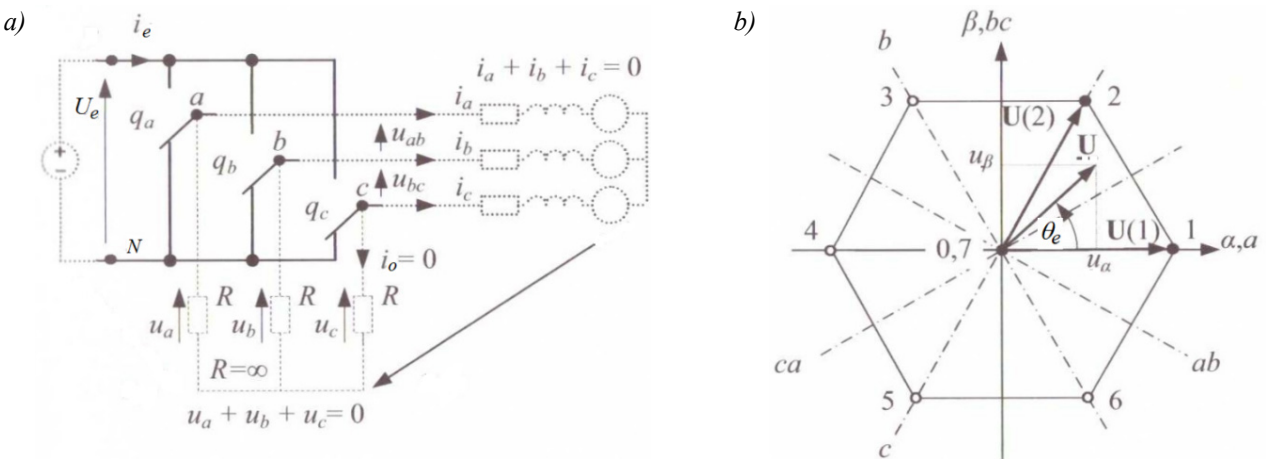

Fig. 5. Diagram of an exemplary three-phase bridge converter and a graph of spatial voltage vector [7]

There are many modulation methods for three-phase converters, which are based on selecting the sequence of vectors **U**(k) as a function of the angle θ_e and calculating the duration of each state. One of the methods is presented below.

A model of an inverter with the structure as in Fig. 6 is described by formulas [3]:

$$\begin{aligned} u_a &= \frac{1}{3}(2u_{01} - u_{02} - u_{03}) = \frac{U_e}{3} \sum_{k=-\infty}^{\infty} \sum_{n=1}^{m} (2c_{01n} - c_{02n} - c_{03n}) e^{jk\theta_e}, \\ u_b &= \frac{1}{3}(2u_{02} - u_{03} - u_{01}) = \frac{U_e}{3} \sum_{k=-\infty}^{\infty} \sum_{n=1}^{m} (2c_{02n} - c_{03n} - c_{01n}) e^{jk\theta_e}, \\ u_c &= \frac{1}{3}(2u_{03} - u_{01} - u_{02}) = \frac{U_e}{3} \sum_{k=-\infty}^{\infty} \sum_{n=1}^{m} (2c_{03n} - c_{01n} - c_{02n}) e^{jk\theta_e}, \end{aligned} \tag{3}$$

where:

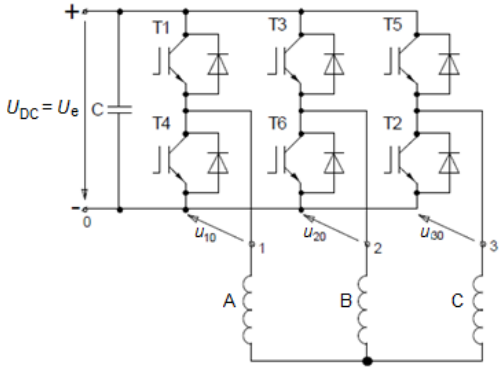

Fig. 6. Three-phase bridge connected inverter [3]

$$u_{01} = \frac{U_e}{2} + r\frac{U_e}{2}\sin(\theta_e),$$
$$u_{02} = \frac{U_e}{2} + r\frac{U_e}{2}\sin\left(\theta_e - \frac{2\pi}{3}\right), \tag{4}$$
$$u_{03} = \frac{U_e}{2} + r\frac{U_e}{2}\sin\left(\theta_e + \frac{2\pi}{3}\right),$$

r – DC voltage regulation coefficient, which equals the ratio of the expected voltage amplitude to the DC, input (power supply) voltage,

m – modulation coefficient; when it is high enough, the difference between real and discrete values is irrelevant,

U_e – DC inverter input voltage.

The output voltage from the inverter for the first phase can be mathematically expressed as a Fourier series:

$$u_{01} = U_e \sum_{k=-\infty}^{\infty} \sum_{n=1}^{m} c_{01n} e^{jk\theta_e}, \tag{5}$$

$$c_{01n} = \frac{1}{j2k\pi}\left(e^{-jk\alpha_{01n}} - e^{jk\beta_{01n}}\right) \quad \text{for} \quad k \neq 0, \tag{6}$$

$$c_{01n} = \frac{\beta_{01n} - \alpha_{01n}}{2\pi} \quad \text{for} \quad k = 0. \tag{7}$$

Similarly:

$$u_{02} = U_e \sum_{k=-\infty}^{\infty} \sum_{n=1}^{m} c_{02n} e^{jk\theta_e}, \tag{8}$$

$$u_{03} = U_e \sum_{k=-\infty}^{\infty} \sum_{n=1}^{m} c_{03n} e^{jk\theta_e}, \tag{9}$$

and phase-to-phase voltages:

$$u_{12} = u_{01} - u_{02} = U_e \sum_{k=-\infty}^{\infty} \sum_{n=1}^{m} (c_{01n} - c_{02n}) e^{jk\theta_e}, \tag{10}$$

$$u_{23} = u_{02} - u_{03} = U_e \sum_{k=-\infty}^{\infty} \sum_{n=1}^{m} (c_{02n} - c_{03n}) e^{jk\theta_e}, \tag{11}$$

$$u_{31} = u_{03} - u_{01} = U_e \sum_{k=-\infty}^{\infty} \sum_{n=1}^{m} (c_{03n} - c_{01n}) e^{jk\theta_e}. \tag{12}$$

Taking into account the Clarke transformation:

$$u_\alpha = \frac{1}{3}(2u_a - u_b - u_c) = \frac{U_e}{3} \sum_{k=-\infty}^{\infty} \sum_{n=1}^{m} (2c_{01n} - c_{02n} - c_{03n}) e^{jk\theta_e}, \tag{13}$$

$$u_\beta = \frac{1}{\sqrt{3}}(u_b - u_c) = \frac{U_e}{\sqrt{3}} \sum_{k=-\infty}^{\infty} \sum_{n=1}^{m} (c_{02n} - c_{03n}) e^{jk\theta_e}. \tag{14}$$

The above transformations can be used to build control systems as in Fig. 7 and 8. In both cases, the motor model in the coordinates dq and PI controllers in the i_d and i_q current circuits were used. They differ in the way of determining the values of currents and adequate voltages.

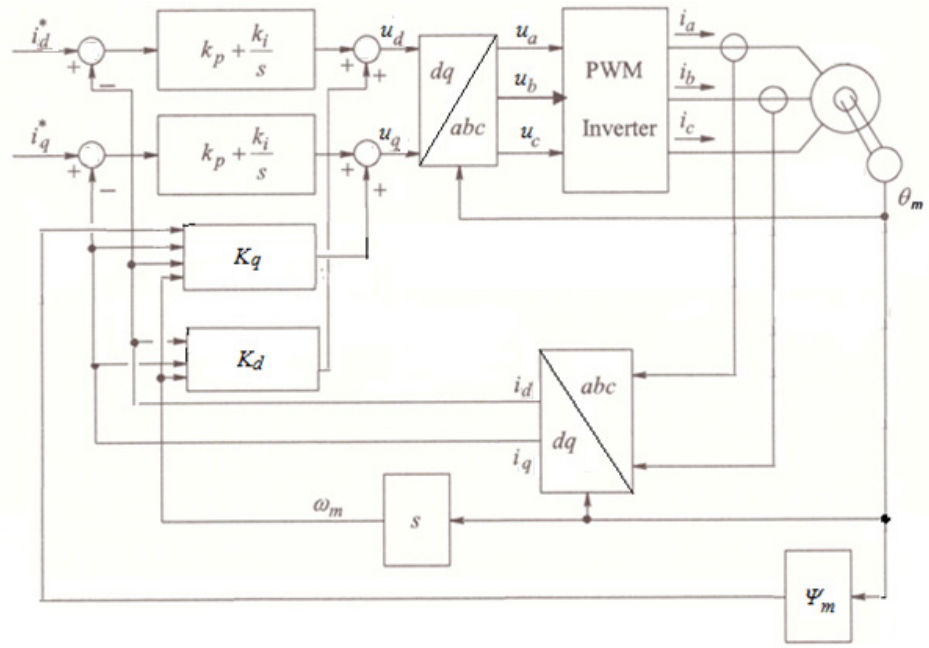

Fig. 7. Schematic diagram of the motor control algorithm according to [4]

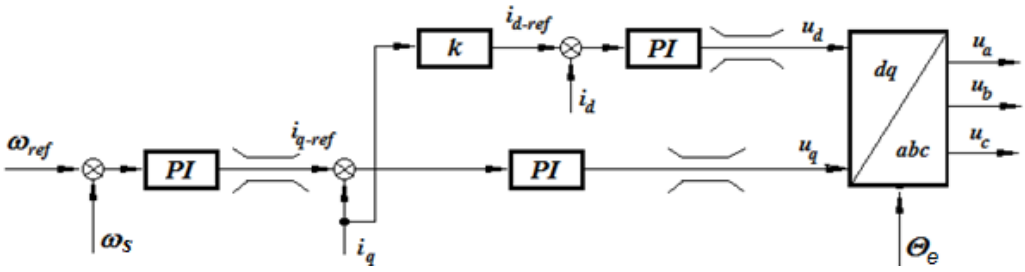

Fig. 8. Block diagram of the control algorithm, according to [9]

The following symbols have been introduced in the diagram above:

$$u_{do} = R_s i_d - L_q p\omega_s i_q + L_d \frac{\mathrm{d}i_d}{\mathrm{d}t} = K_d + L_d \frac{\mathrm{d}i_d}{\mathrm{d}t},$$
$$u_{qo} = R_s i_q + p\omega_s \left(L_d i_d + \psi_m\right) + L_q \frac{di_q}{dt} = K_q + L_q \frac{di_q}{dt}. \tag{15}$$

As shown in Fig. 7, the transformation of signals in two directions is used in the control system:

– in the direction $dq \rightarrow abc$:

$$\begin{bmatrix} u_a \\ u_b \\ u_c \end{bmatrix} = \sqrt{\frac{2}{3}} \begin{bmatrix} \cos(\theta_e) & -\sin(\theta_e) \\ \cos\left(\theta_e + \frac{4\pi}{3}\right) & -\sin\left(\theta_e + \frac{4\pi}{3}\right) \\ \cos\left(\theta_e + \frac{2\pi}{3}\right) & -\sin\left(\theta_e + \frac{2\pi}{3}\right) \end{bmatrix} \begin{bmatrix} u_d \\ u_q \end{bmatrix}, \tag{16}$$

– and in the reverse direction $abc \rightarrow dq$:

$$\begin{bmatrix} i_d \\ i_q \end{bmatrix} = \sqrt{\frac{2}{3}} \begin{bmatrix} \cos(\theta_e) & \cos\left(\theta_e - \frac{2\pi}{3}\right) & \cos\left(\theta_e - \frac{4\pi}{3}\right) \\ -sin(\theta_e) & -\sin\left(\theta_e - \frac{2\pi}{3}\right) & -\sin\left(\theta_e - \frac{4\pi}{3}\right) \end{bmatrix} \begin{bmatrix} i_a \\ i_b \\ i_c \end{bmatrix}. \tag{17}$$

PI controllers (Fig. 7) directly affect the changes of fluxes connected with the inductances in the q-axis and the d-axis.

In the algorithm shown in Fig. 8, the signal ω_{ref} given by the driver and the actual velocity ω_s differ from each other. This error, after passing the PI controller, is the set value of current $i_{q\text{-}ref}$ for the adder in the *d*-axis. There are limiters at the output of the i_d and i_q current controllers. The voltages, which were predetermined in the *dq* system, are transformed into a system of stationary coordinates *a*, *b*, *c* after passing the controllers and the limiters. The measured instantaneous angle θ_m, converted into the electrical angle θ_e, was taken into account while determining the voltages in the *dq* system.

Comparing the algorithms presented in Fig. 7 and 8, one can notice their high compatibility in the structure.

2. Sample results

A sample model of a motor with an inverter is shown in Fig. 9. Two regulation loops are proposed here: we can regulate either the angular velocity of the motor shaft (vehicle velocity) or the torque, but the i_d and i_q current loops or the $i_{a,b,c}$ phase current loops are also possible.

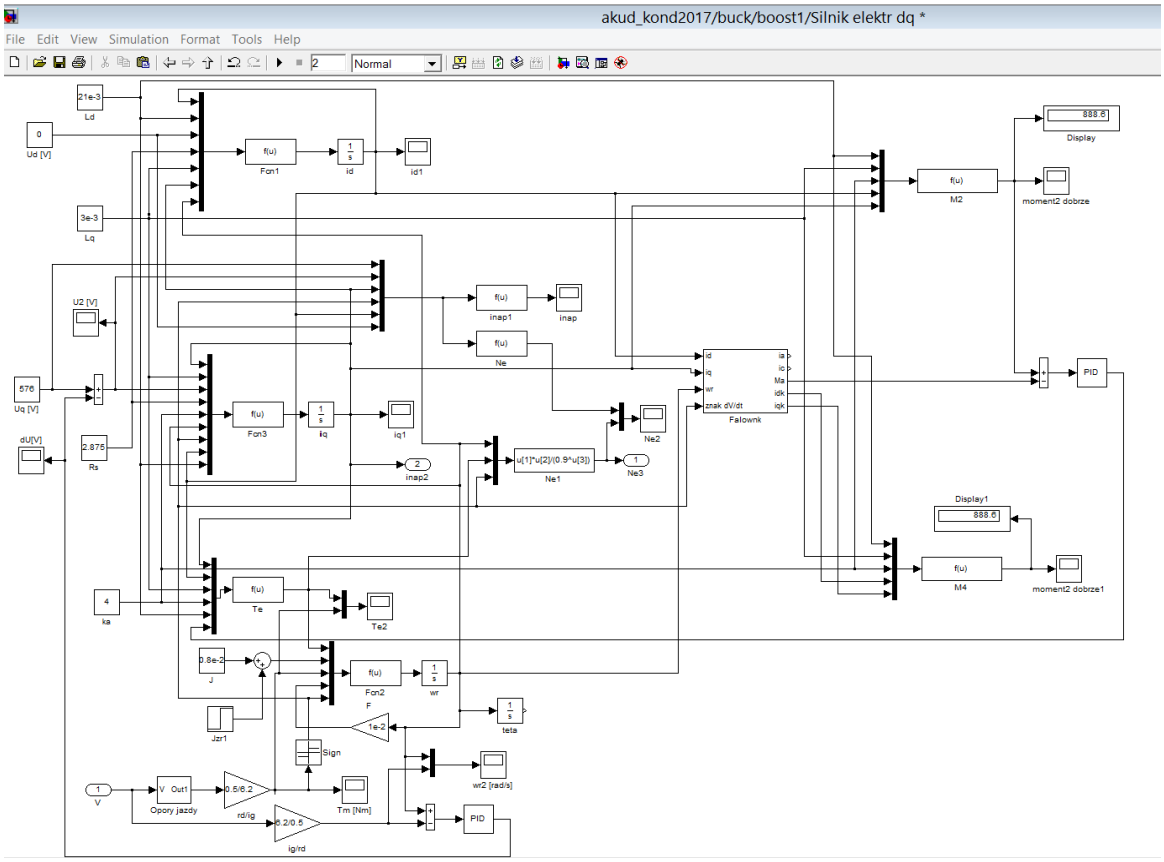

Fig. 9. Model of a motor with an inverter

The model and the waveforms $i_{a,b,c}$, shown in Fig. 10 and 11, are the result of mathematical relations previously discussed. The amplitude values of phase currents correspond to the torque at the motor shaft. The initial period of 2 seconds is shown in Fig. 11 to analyse the phase shift.

Figures 12 and 13 depict PWM signals determined according to the diagram shown in Fig. 2.

Examples of determining operating states of switches in a three-phase inverter according to the scheme from Fig. 5 are shown in Fig. 14 and 15. The presented control signals are only special cases of vector modulation, indicating what tasks, resulting from the above formulas and descriptions, must be done by the software ("overlay") of commercial inverters.

An overview of modulation methods can be found in the extensive literature on converters.

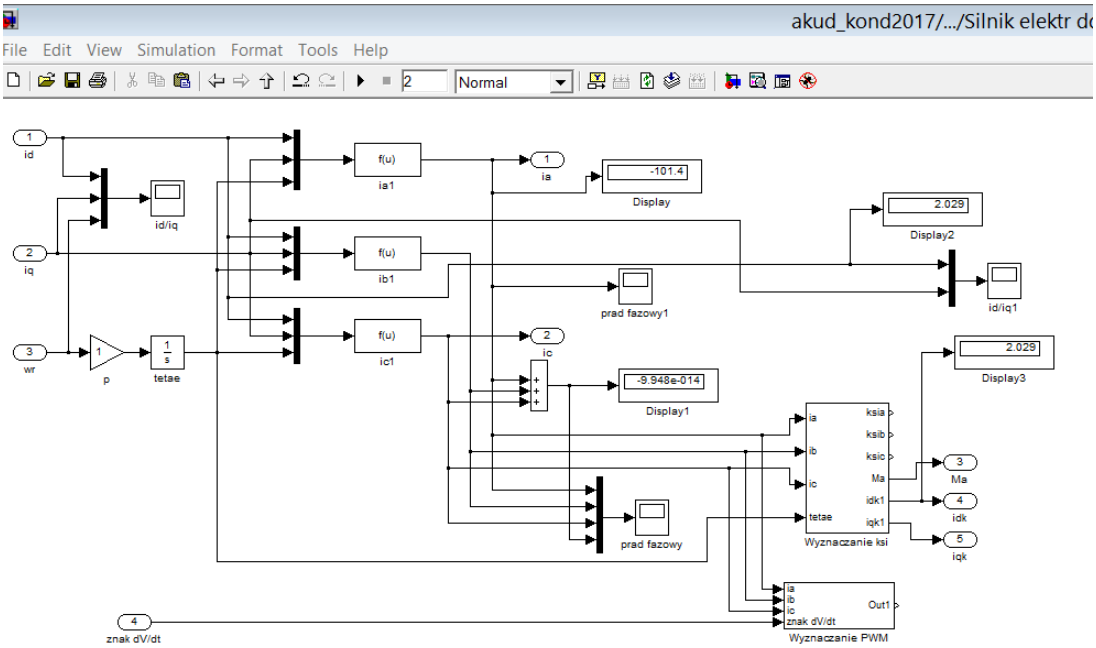

Fig. 10. Inverter model – determination of phase currents and stator flux linkages

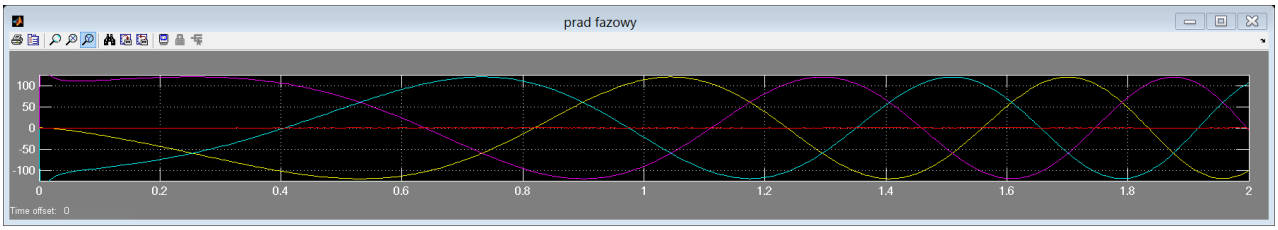

Fig. 11. Phase currents $i_{a,b,c}$

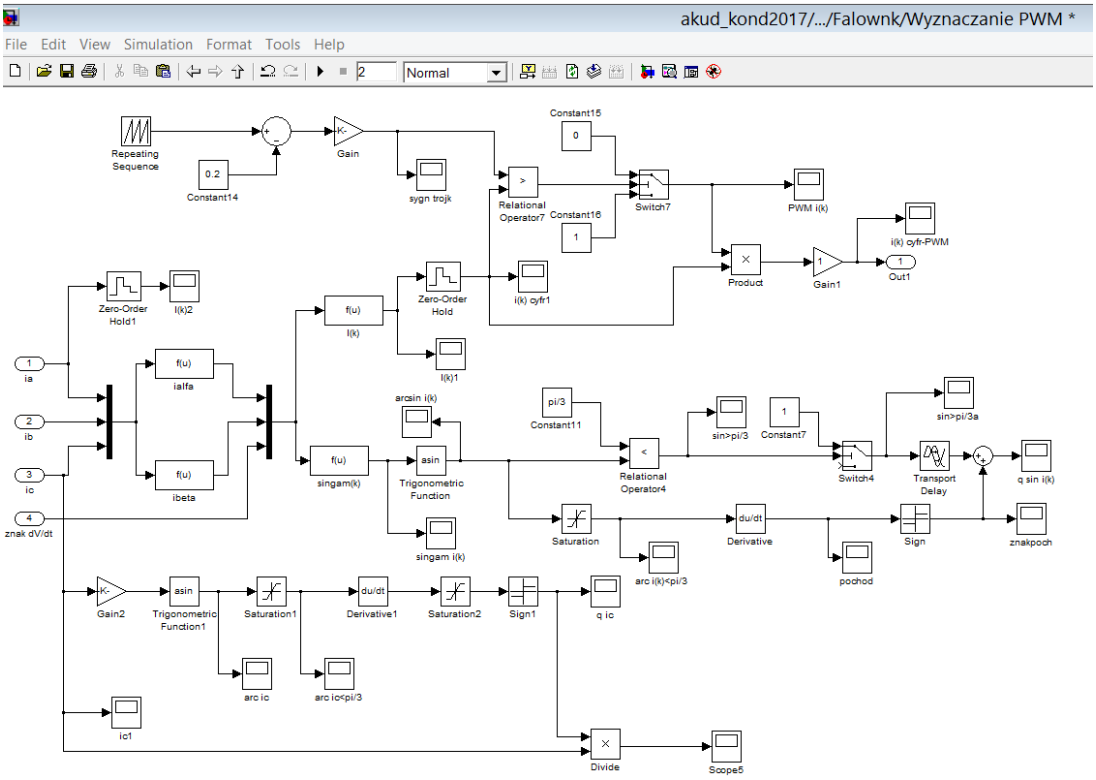

Fig. 12. Inverter model – determination of PWM signals for phase currents and stator flux linkages

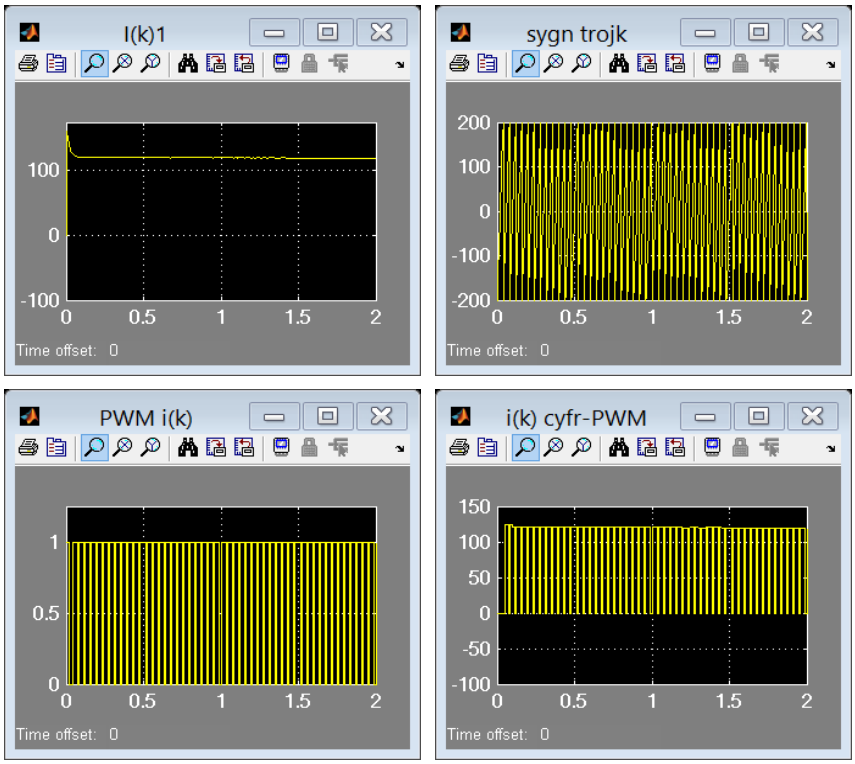

Fig. 13. Inverter model – determination of spatial current

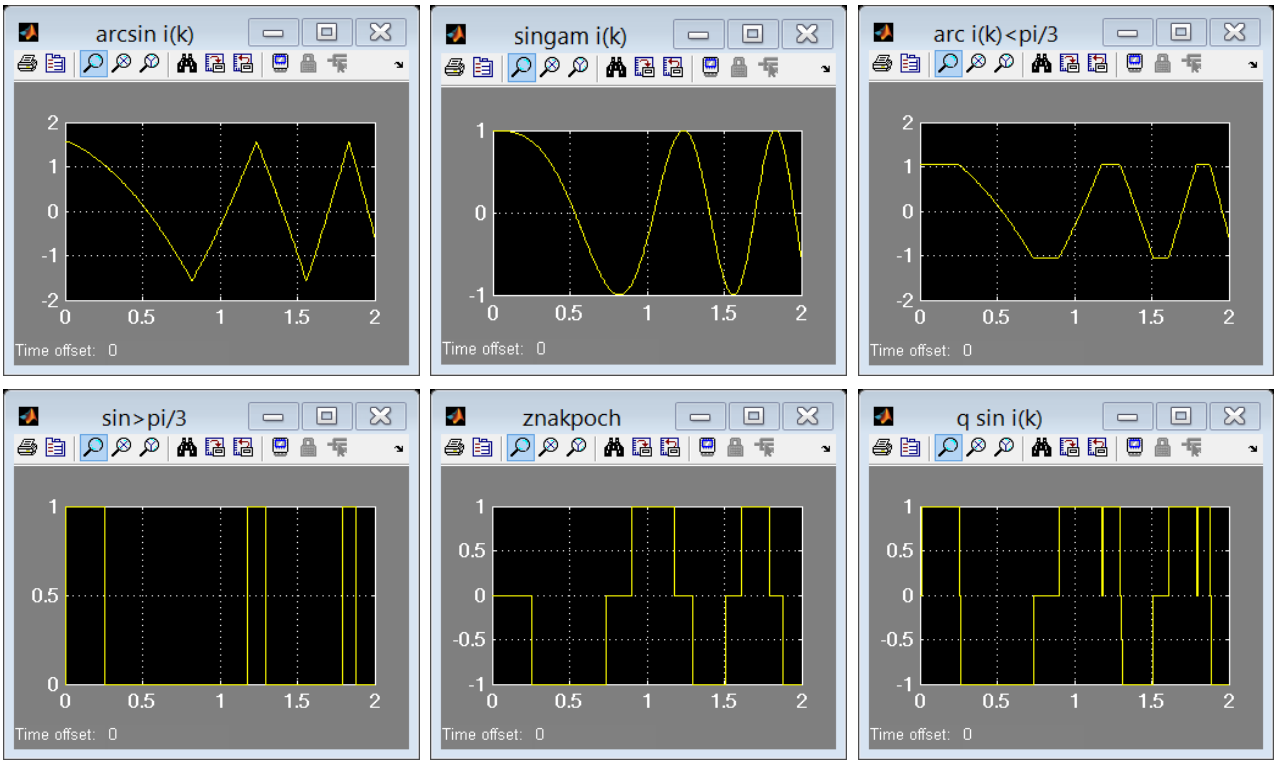

Fig. 14. Inverter model – determination of operating states (qik) of switches for spatial current

3. Conclusions

The presented relations describing motor and inverter models allow development of control algorithms for electric drives in various configurations, even at the stage of theoretical considerations. It is obvious that the algorithm should take into account also the system of protection

against overloads, e.g. electrical and temperature overloads that may occur in the electrical system. Many of these elements already exist in the default software of inverters and hence the "insight" in the algorithm of the inverter is necessary for proper configuration of the so-called "overlay".

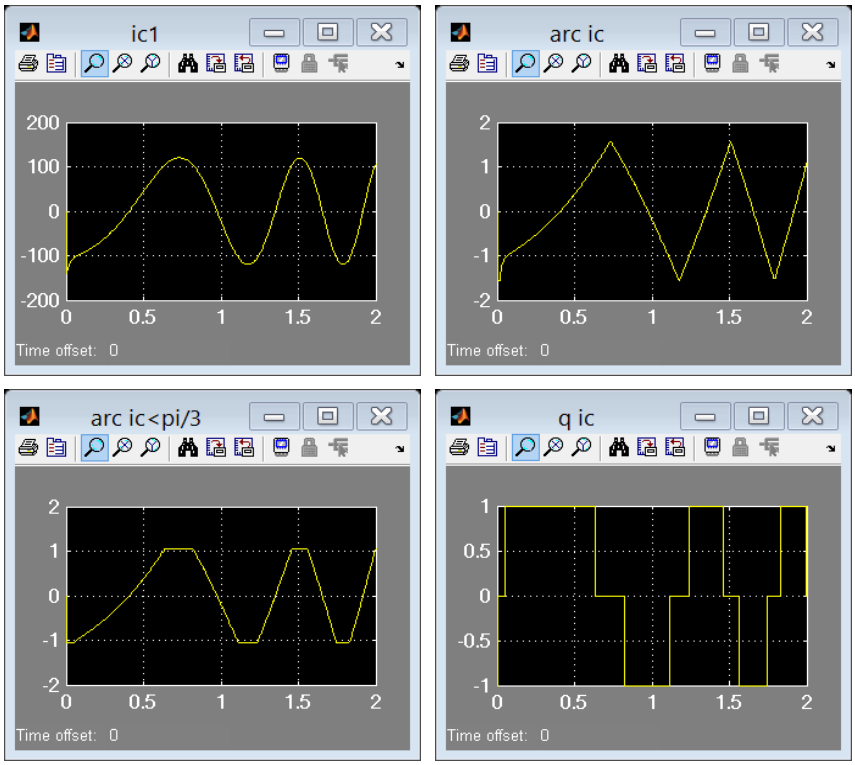

Fig. 15. Inverter model – determination of the operating state q_{ic} of switches for the phase current i_c

For vector control, the mathematical model of a synchronous machine in the *dq* coordinate system is the most common one. The most important feature of this control method is the fact that the i_q component of the rotor current vector determines the value of motor torque, and the component i_d – the value of magnetic flux.

In reality, there is a magnetic asymmetry and, if it is to be taken into consideration, it requires a more elaborate trapezoidal model in phase coordinates, in which the flux from permanent magnets generates trapezoidal courses with a coupling (EMF). In this case, a mathematical description in natural coordinates is used.

In the article, the emphasis is put on how inverters work. Their basic task is to generate such currents i_{abc} or voltages u_{abc} to obtain torque without ripples. It leads to development of different control concepts for achieving this goal, which are related to the modelling of magnetic fluxes in a stator and in an inverter.

References

[1] Lis, M., Makarchuk, O., *Model matematyczny elektromechanicznych stanów nieustalonych silnika typu BLDC zasilanego ze źródła napięcia sinusoidalnego*, Maszyny Elektryczne, No. 1, pp. 183-188, 2013.

[2] Lis, M., Makarchuk, O., *Model matematyczny silnika synchronicznego z magnesami trwałymi o sterowaniu sinusoidalnym zasilanego ze źródła prądowego*, Maszyny Elektryczne, No. 3, pp. 175-178, 2012.

[3] Zaskalicky, P., *Calculation of a torque ripple a three-phase asynchronous motor supplied by a PWM controlled inverter*, Maszyny Elektryczne, No. 2, pp. 53-58, 2014.

[4] Mohan, N., *Advanced Electric Drives*, Wiley&Sons, 2014.

[5] Shchur, I., Rusek, A., Makarchuk, O., *Modelowanie symulacyjno-komputerowe silnika synchronicznego z magnesami trwałymi na podstawie wyników badań polowych*, Maszyny Elektryczne, No. 3, pp. 189-195, 2012.
[6] *Matlab-simulink, Biblioteka oprogramowania MATLAB*.
[7] Zawirski, K., Deskur, J., Kaczmarek, T., *Automatyka napędu elektrycznego*, Wydawnictwo Politechniki Poznańskiej, Poznan 2012.
[8] Czaban, A., Czaban, W., Rusek, A., Lis, M., *Model matematyczny silnika synchronicznego z magnesami trwałymi typu PMSM z wykorzystaniem metod wariacyjnych*, Maszyny Elektryczne, No. 1, pp. 177-181, 2013.
[9] Załęski, J., Dadana, M., Młodzikowski, P., Twerd, M., *Przekształtnikowy napęd samochodu elektrycznego*, Maszyny Elektryczne, No. 1, pp. 89-93, 2013.
[10] Król, E., Rossa, R., *Silnik synchroniczny z magnesami trwałymi jako napęd pojazdu hybrydowego*, Zeszyty Problemowe – Maszyny Elektryczne, No. 4, pp. 71-74, 2012.
[11] Giurgiutiu, V., Lyshevski, S. E., *Micromechatronics. Modeling, Analysis, and Design with MATLAB*, CRC Press by Taylor & Francis Group, LLC, 2009.
[12] Pawelski, Z., Zdziennicki, Z., *Model of vehicle electric drive system*, Journal of KONES Powertrain and Transport, Vol. 24, No. 3, pp. 211-220, 2017.

Manuscript received 03 July 2018; approved for printing 04 October 2018